

Deformation analysis of railgun cross-section

P. Gildutis*, R. Kačianauskas**, M. Schneider***, E. Stupak****, R. Stonkus*****

*Vilnius Gediminas Technical University, Saulėtekio 11, 10223 Vilnius, Lithuania, E-mail: paulius.gildutis@vgtu.lt

**Vilnius Gediminas Technical University, Saulėtekio 11, 10223 Vilnius, Lithuania, E-mail: rkac@vgtu.lt

***French-German Research Institute of Saint Louis (ISL), 5 rue G'al Cassagnou, 68301 Saint-Louis, France, E-mail: schneider_m@isl.tm.fr

****Vilnius Gediminas Technical University, Saulėtekio 11, 10223 Vilnius, Lithuania, E-mail: Eugenius.Stupak@vgtu.lt

*****Vilnius Gediminas Technical University, Saulėtekio 11, 10223 Vilnius, Lithuania, E-mail: ma@vgtu.lt

crossref <http://dx.doi.org/10.5755/j01.mech.18.3.1877>

1. Introduction

Electromagnetic accelerators cover a wide range of applications. They can be used to accelerate very large masses up to modest velocities below 100 m/s (e.g. aircraft launch systems, [1]) and there exist also accelerator types, which are able to accelerate small masses (some grams) up to more than 6 km/s [2]. This article deals with an accelerator type, known in the literature as railgun, which works in the range from several hundred grams up to some kilograms and reaches velocities in excess of 2 km/s. Research on railguns has a strong multidisciplinary character including electromagnetic, thermal and mechanical phenomena. Enormous current densities, high velocities of moving forces coupled with the dynamical interaction at the rail surface present a great challenge. Advances in electromagnetic launch science and technology can be found in review papers [3, 4].

A typical railgun facility comprises the accelerator, the projectile including a conducting armature and an electric energy source. The electric circuit is formed by the source, the rails and the sliding contact between the latter realized by the armatures. The strong currents used result in strong Lorentz forces on conducting materials, in particular the projectile is accelerated by the Lorentz-force acting on the armatures. It is guided by the rails in one direction and by insulating parts in the other (see below). The rails have to withstand strong repelling Lorentz forces. Experimentally realized railgun setups differ with respect to the structure of the rails and the housing [5, 6].

The mechanical response of the railgun structure to the magnetic forces acting on the rails became recently one of the biggest challenges encountered in designing and researching electromagnetic railguns, because rail deformation can influence the crucial sliding contact performance of the armature. Therefore, evaluation of the deflections of the inner rail surfaces considered hereafter is a mandatory task for future systems.

However, in order to investigate the rail deformation, the electromechanic problem can be decoupled into a mechanical one and an electromagnetic one. The electromagnetic forces enter the mechanical calculations in form of boundary conditions [7].

The transient elastic waves in electromagnetic launchers and their influence on armature contact pressure were studied by Johnson and Moon [8, 9]. Actually, in their coupled rail-armature FE model the rail was considered as a beam, while the armature was discretized by quadrilateral elements.

Probably, the simplest model treats the rail as one-dimensional beam on an elastic foundation. Analytical treatment of the beam under moving point loads and the simplest solutions are presented in the book by Fryba [10]. An analytical approach to investigate the dynamic response of laboratory railguns including projectile movement was developed in series of works by Tzeng [11] and Tzeng and Sun [12]. The rail was modelled as cantilever beam on an elastic foundation.

It is obvious that a better understanding of the structural behaviour of the railgun can be achieved through modelling and computer simulation, as it enables to obtain detailed quantitative information. In particular, numerical investigations using the Finite Element Method (FEM) has become a routine in recent decades. In the ideal case, an electromechanically coupled 3D finite element model would be appropriate.

It is worth to notice, that the use of the 3D solid FE models in the multifield analysis is very expensive and not always reasonable. Consequently, a balance between the accuracy and the cost should be found.

Transient resonance at critical velocities of the projectile was numerically studied by Lewis and Nechitailo [13]. There, axis-symmetric shell and two-dimensional solid models were used to simulate the railgun presented in the form of a tube.

Electromagnetic launchers have been extensively investigated at the French-German Research Institute of Saint-Louis (ISL), where specific types of railguns, characterized by the use of discrete supports, have been developed [14, 15]. In order to withstand the high forces repelling the rails from each other, the housing consists of a combination of bars of glass fiber reinforced plastic (GRP) material and symmetrically located steel bolts representing the discrete supports.

At present time, research on electromagnetic devices is continued in cooperation with the Vilnius High Magnetic Field Centre, Lithuania [16]. Here, various applications of the FEM including linear actuators [17], destructive coils [18, 19] were considered.

Dynamic behaviour of the ISL railgun EMA3 under uniformly distributed load moving with various velocities was studied in [20-23]. Therewith, a longitudinal 2D plane stress finite element model, resting upon discrete elastic supports, was developed to represent the complex bar. The model is able to capture bending and shear effects described conventionally by beam models, as well as pinching deformation of the solid cross-section.

This paper presents the first results in a series of

research efforts aiming to perform numerical modelling of the electromagnetic gun RAFIRA (RAPid Fire RAilgun) [24, 25] of ISL. The development of a reliable simplified FE model is the final goal of this investigation. This paper deals with the understanding and the illustration of cross-sectional deformation behaviour under static and dynamic loading.

The outline of the paper is as follows. Section 2 presents the description of the rail gun problem. Section 3 describes the modelling approach. Numerical results are discussed in section 4. Conclusions are drawn in sections 5 and 6.

2. Railgun - structure and basic data

The ISL - railgun RAFIRA has an acceleration length L of 3.1 m. A schematic 3D view of the railgun structure is presented in Fig. 1. The whole structure is designed to withstand the high forces repelling the rails from each other during the motion of the projectile between the rails. The barrel consists of two bars of rectangular section connected with 160 steel bolts M18, which are located in four rows as shown in Fig. 1. The bolts are inserted into the insulators, which are manufactured from electrically nonconductive composite materials and stowed among the bar. Rails are fixed to the frame with hexagonal bolts.

The view and the main data of cross-section A-A presented in Fig. 2. Here, all lengths are given in millimeters. The height of section is $H = 225$, the width $W = 200$. The section of the bar is defined by the width which is equal to W , while the height is $h = 80$. The M18 bolt is defined by diameter $D = 18$ and the washer by diameter $d = 36$. The section of the rail is defined by width $W_R = 25$ and height $H_R = 20$. The bolt location is described by value $S_d = 27.5$.

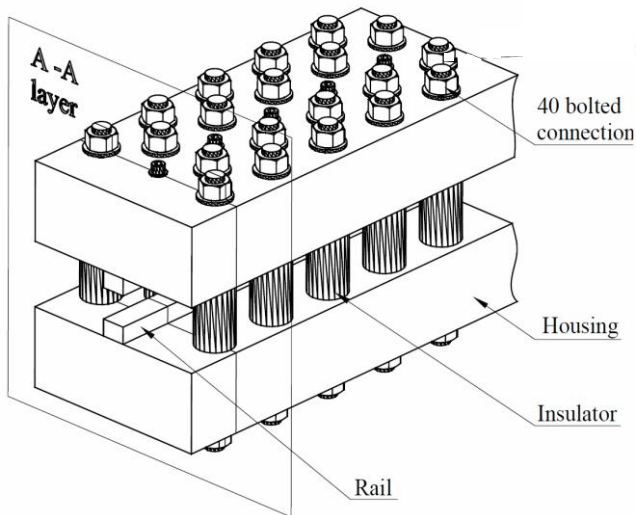


Fig. 1 Schematic three-dimensional view of railgun

Materials and their mechanical characteristics of individual parts of the mechanism are the same as the EMA-3 railgun [20]: bolt manufactured from steel alloy (density $\rho_{bolt} = 7.85 \text{ g/cm}^3$, elasticity modulus $E_{bolt} = 210 \text{ GPa}$, Poisson's ratio $\nu_{bolt} = 0.30$), rail - copper-chromium-zirconium alloy, CuCr1Zr ($\rho_{rail} = 8.90 \text{ g/cm}^3$, $E_{rail} = 120 \text{ GPa}$, $\nu_{rail} = 0.30$), bar - from composite, EPM 203 ($\rho_{bar} = 1.85 \text{ g/cm}^3$, $E_{bar} = 18.0 \text{ GPa}$, $\nu_{bar} = 0.30$).

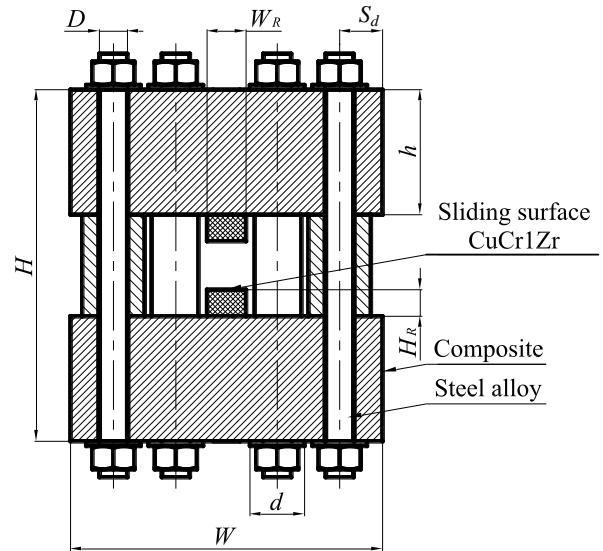


Fig. 2 Cross-section A-A of railgun

3. FE model and analysis

As mentioned above, the structural analysis of the railgun system can be decoupled from electromagnetic phenomena at the first stage and therefore purely mechanical calculations are to be performed. The railgun housing dynamics will also be treated as being independent from the projectile behaviour. Considering plane symmetry of the barrel, only one half of its cross-section can be investigated. Thus, the load carrying structure of the railgun presents solid slender bar while fastening bolts may be treated as discrete elastic supports.

It is commonly agreed that the deflections of the sliding surface is a consequence of the complex interaction of various deformation modes. Therefore, contributions of the global longitudinal deformation modes are assumed to be dominating in the total response of the whole structure. The one-dimensional beam with undeformable cross-sections applied in the earliest developments [22] is an example for a purely global approach.

In reality, the transversal distortion of the cross-section is generally of 3D nature. To avoid the detailed three-dimensional analysis further simplifications could be used.

Our suggestion is based on the assumed orthogonality of longitudinal and transversal deformation modes. Taking into account the length and size ratio $L/W = 3.1/0.2 = 15.5$ transversal deformation is considered as plane strain problem. Consequently, the T-shaped bimaterial cross-section of the bar-prism will be treated as 2D solution domain.

The computational model of the railgun section applied hereafter for static and transient analysis is shown in Fig. 3. The sketch shows a vertically symmetric composition of two rectangles, the bar and the rail. The bar section is defined as $W \times h = 200 \times 80 \text{ mm}^2$ while the rail is characterized as $W_r \times H_r = 25 \times 20 \text{ mm}^2$.

Two section bolts are considered as elastic supports. To avoid local concentration in connection, each of bolts has been replaced by the set of five identical elastic springs with length equal to a half of the section height $H/2 = 112.5 \text{ mm}$ as shown in Fig. 2. Location of the middle spring coincides with the central axis of the bolts and de-

finied by distance $S_d = 27.5$. The remainder four springs are uniformly located across the diameter d of the bush-washing with distance $d/4 = 9$ mm from each other.

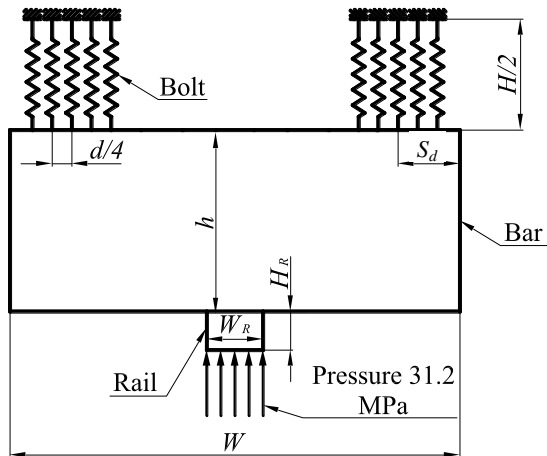


Fig. 3 Computational model of the Railgun section

The loading of the structure corresponds to the magnetic pressure caused by the strong currents following the moving projectile, while local transversal contact forces caused by the projectile (armature) are neglected. As a result, the transient loading profile represents the magnetic pressure $q(x, t)$ at an arbitrary point x moving in time t with the velocity $v(t)$. In the static case a constant pressure $q = \text{const}$ is assumed.

Numerical simulation is carried out using the FEM program ANSYS [26]. Two-dimensional domains comprising the rail and the bar are covered by 8 node plane finite elements - Plane183 with 2 DOF per node. The element contains large deflection, large strain and dynamic capability.

The spring type Link1 finite elements with 2 DOF per node are applied for modelling of bolts. The element contains not only linear but also large deflection capabilities. The spring elements are connected to a rigid plane while spring-structure connection nodes are constrained in horizontal x direction. The axial stiffness of the spring assembly reflects stiffness of the entire bolt as a whole. Available deformation of the bolt threads [27] is not taken into account. Distributed springs additionally evaluate the local bending of the bolts. Finally, each of individual spring is defined by the section area equal to $5.6677 \times 10^{-5} \text{ m}^2$.

A combined irregular-structured automatically generated FE mesh was used. To test the influence of the mesh density, a convergence study was performed. The five meshes denoted by Mesh 1 up to Mesh 5 with 178, 275, 579, 1594 and 4836 finite elements were examined. The coarsest and the densest mesh are given in Fig. 4. The locations of the supports are fixed and remain independent from the mesh refinement.

During the convergence test, a static pressure $p = 31.2$ MPa is applied on the inner surface of the rail as it is shown in Fig. 3. The maximal displacement of the point S on the sliding surface u_S is chosen as convergence criterion and examined below. It comprises displacement due to local deformation of the structure and due to elongations of the bolts.

Simulation results of static loading cases are pre-

sented in Table 1. As expected, elongations of bolts expressed by the displacement of the support u_A do not depend on the mesh density. In summary, a relatively coarse mesh seems to be sufficiently accurate to describe the deformation behaviour of the cross-section.

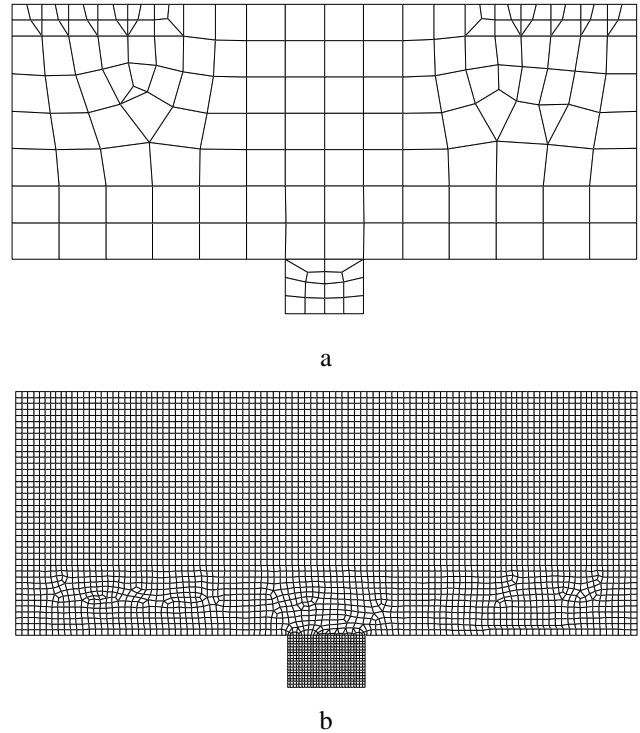


Fig. 4 Finite element meshes: a coarse mesh with 178 plane elements, b - densest mesh with 4863 elements

Table 1
Displacements of railgun under various density of mesh

| Parameters | Mesh 1 | Mesh 2 | Mesh 3 | Mesh 4 | Mesh 5 |
|-------------------------------|--------|--------|--------|--------|--------|
| Number of plane elements | 178 | 275 | 579 | 1594 | 4836 |
| Number of DOF | 1116 | 1738 | 3626 | 9086 | 29632 |
| Total displacement u_S , mm | 0.832 | 0.832 | 0.833 | 0.835 | 0.837 |
| u_A , mm | 0.735 | 0.735 | 0.735 | 0.735 | 0.735 |

Since the results obtained for various mesh densities do not differ significantly, further calculations we made using the numerical model with 579 finite elements.

4. Investigation of static loading

The main aim of the study presented here is the investigation of the transversal deformation modes which were neglected in the previously published works [18-21]. Hypothetical statements about the possible deformation modes were suggested and three deformation modes were examined. They are:

- deformation of the elastic support defined as elongation of bolts;

- transversal bending;
- axial deformation (pinching) of the section under compression.

In order to characterise the deformation behaviour of the sliding surface notation Δ will be employed hereafter to characterise the deformation behaviour. The total deformation of the section which characterises displacement of the sliding surface is defined by displacement of the central point S : $\Delta_{total} = u_S$ (Fig. 5). The displacement u_s as well as in other points are extracted from the FE computations.

It is evaluated as result of the three deformation modes mentioned above plus an error term Δ_{err} reflecting possible undefined effects. Explicitly, the displacement of S becomes

$$\Delta_{total} = \Delta_{bolt} + \Delta_{bend} + \Delta_{bar} + \Delta_{rail} + \Delta_{err} \quad (1)$$

The elongation of the bolt Δ_{bolt} is simply defined by displacement of the central point A (2) of the support as

$$\Delta_{bolt} = u_A \quad (2)$$

The axial deformation (pinching) of the rail and bar sections can be defined by displacement differences of the points B , C and S as

$$\left. \begin{aligned} \Delta_{rail} &= u_S - u_C \\ \Delta_{bar} &= u_C - u_B \end{aligned} \right\} \quad (3)$$

Transversal bending is characterised by deflection of the plane section assumed to be simply supported beam. It could be measured by deflection w_B of the point B (4). Finally, the displacement of the sliding surface due to transversal bending Δ_{bend} may be extracted as

$$\Delta_{bend} = w_B = u_B - u_A \quad (4)$$

Linear and nonlinear large displacement analysis problems were considered under action of static pressure $p = 31.2$ MPa applied in the simulation.

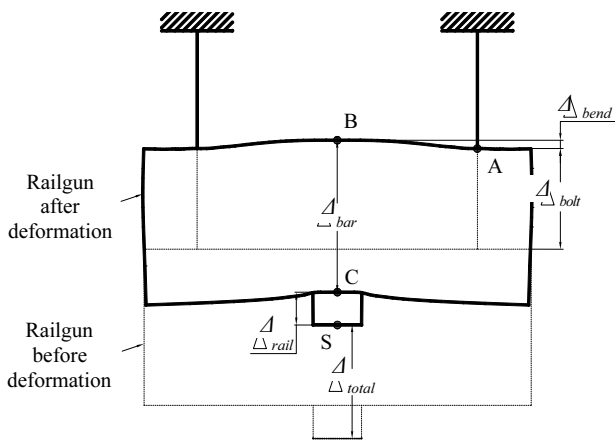


Fig. 5 Schematic deformation of the railgun cross section

Results of a linear static simulation are graphically presented in Fig. 6.

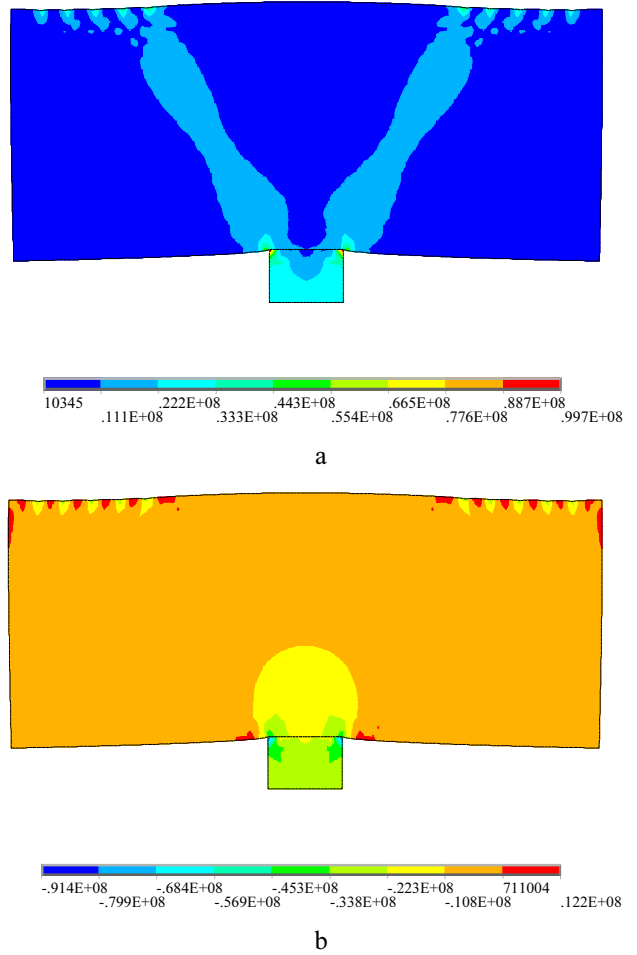


Fig. 6 Deformed shape and contour plots under static loading (in Pa): a) von Mises stress and b) normal vertical stress

To understand the deformation behaviour of the section, the linear and geometrically nonlinear static analysis was performed. Contributions of the deformation modes according to expressions (1) - (4) were analysed while results of linear and nonlinear static analysis are compared in Table 2 and graphically illustrated in Fig. 7. The first observation is that differences between both approaches are insignificant. Results confirm that because of the high stiffness of the bars the influence of geometric nonlinearity, i.e. of deformed shape, is negligibly small.

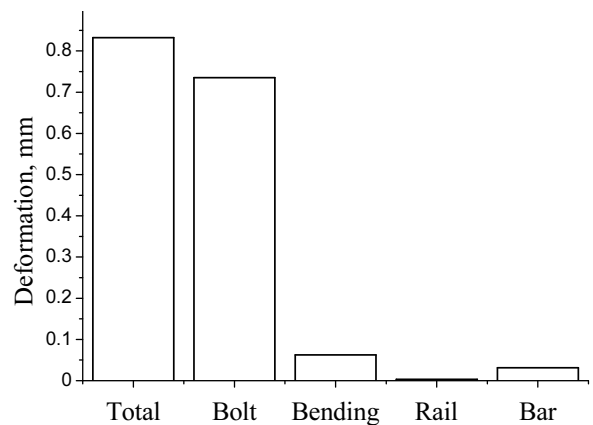


Fig. 7 Comparative illustration of section displacements

Table 2
Contributions of various deformation modes to sliding surface displacement obtained by static analysis

| Deformation mode | Displacements, mm | | Relative contribution |
|------------------|-------------------|-----------|-----------------------|
| | Linear static | Nonlinear | |
| Δ_{total} | 0.833 | 0.833 | 100% |
| Δ_{bolt} | 0.735 | 0.735 | 88.2% |
| Δ_{bend} | 0.06289 | 0.06273 | 7.5% |
| Δ_{rail} | 0.00367 | 0.00314 | 0.5% |
| Δ_{bar} | 0.03144 | 0.03144 | 3.8% |

Moreover, the data clearly shows that the largest, approximately 88%, contribution of the sliding surface displacement is due to the elongation of bolts while the influence of transversal bending comprising 7.5% is also important.

Simulation results processed according to expression (3) clearly demonstrate the contribution of the axial deformation of the section structure under compression. On the other hand, variation of the normal stresses shown in Fig. 6 demonstrates 2D character which can not be explained by simple compression. Mechanical interpretation of this effect will be given below. Theoretically, normal deformation of the section Δ_{BS} , i.e. change of the distance between points B and S, may be evaluated as

$$\Delta_{BS} = \Delta_{bar,t} + \Delta_{rail,t} + \Delta_{int} \quad (5)$$

The above terms comprise contributions of the rail $\Delta_{rail,t}$ and the bar $\Delta_{bar,t}$. The third term Δ_{int} indicates interpenetration of the rail into the bar because deformation of contacting layers.

The first two terms of Eq. (5) can be evaluated analytically as elongation of the axially compressed rod

$$\Delta_{rail,t} = \frac{pW_r \times 1 \times H_r}{E_{rail}W_r \times 1} \quad (6)$$

$$\Delta_{bar,t} = \frac{pW_r \times 1 \times h}{E_{bar}W \times 1} \quad (7)$$

The interpenetration Δ_{int} is calculated on the basis of numerical results.

Detailed analysis of the section deformation according to Eqs. (5) - (7) shows that the deformation mode characterised as pinching of the bar-rail structure is considerably contributed by interpenetration of the rail into the bar. It was found that $\Delta_{int} = 0.01283$ mm yields about 37% of the bar-rail section deformation $\Delta_{bar,t} + \Delta_{rail,t} = 0.03458$ mm, while its contribution to the total deformation of the whole section comprises up to 1.5% of $\Delta_{total} = 0.833$ mm as given in Table 2. This effect was neglected in the earlier 2D models [20-23].

Finally, it should be noted that the error term Δ_{err} in expression (1) turned out to be negligibly small. This indicates that the chosen deformation model uses the appropriate deformation modes.

5. Dynamic time history analysis

The dynamic time history analysis was performed to consider deformation behaviour of the railgun section. The real loading of the railgun presents a transient pressure profile moving along the sliding surface with the projectile

velocities up to 1600 m/s. The maximal pressure value $p = 31.2$ MPa.

Solving a linear dynamic task, the load is acting on the rail. This load in our model is presented as follows. We assume that the moving maximal pressure crosses a section slice of unit (1 mm) thickness as it used in plane strain analysis. Thus the crossing dynamic load should increase from zero and reaches its maximal value. In our case, the maximal pressure value was reached during 1.25 ms and remains constant. In our model the loading history imitates the shock load which is frozen after reaching its maximum.

Simulation results are presented in terms of displacements. Variation of displacement in time is presented in Fig. 8. Comparisons of maximum values of nonlinear dynamic displacements with static results are given in Table 3.

Table 3
Comparison of various deformation modes to sliding displacement obtained by static and dynamic analysis

| Deformation mode | Max. displacements, mm | |
|------------------|------------------------|-------------------------|
| | Linear static analysis | Linear dynamic analysis |
| Δ_{total} | 0.833 | 1.629 |
| Δ_{bolt} | 0.735 | 1.485 |
| Δ_{bend} | 0.06289 | 0.126 |
| Δ_{rail} | 0.00367 | 0.00359 |
| Δ_{bar} | 0.03144 | 0.01452 |

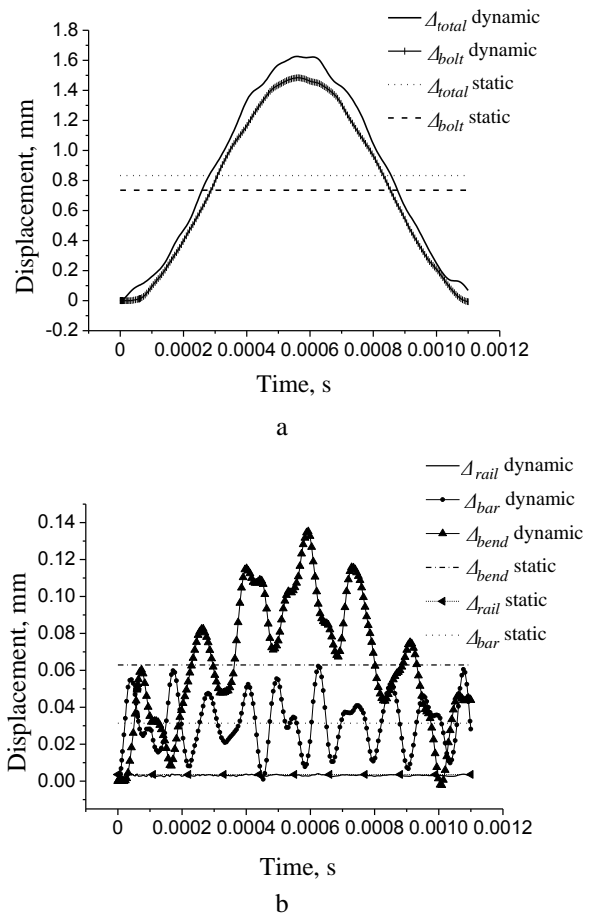


Fig. 8 Time histories of the displacements under dynamic loading: a) total and bolt displacement in Y direction; b) rail, bending and bar displacement

Result shows that dynamic load increase section deformation by the factor approximately equal 2. The relative contribution of various deformation modes approximately equivalent to the static behaviour.

On the other hand, time variation illustrate that each deformation mode are characterised by difference in period, therefore detailed frequency analysis is required to understand deformations of the real structure.

6. Concluding remarks

The transversal deformation behaviour of the existing rail gun structure under action of static and dynamic loading was analyzed on the basis of plane strain formulation using the finite element method. The presented results illustrate qualitatively and quantitatively in-plane flexibility of the bar as whole while role of particular deformation modes is clearly distinguished. The most important findings are summarised as follows.

- Normal displacement of the sliding surface due to deformation of section of the entire section is basically attributed to the tension of the bolts providing 88% of the total value. Contribution of the transversal bending characterised by central deflection is of 7.5% while deformation of the bar section under compression contains up to 3.8%.
- Dynamic contribution of moving load is characterised by factor approximately equal 2.

This study forms the base for the future development of a 3D model allowing to investigate the influence of mesh density and particular deformation effects.

References

1. **Doyle, R.; Samuel, D.J.; Conway, T.; Klimowski, R.R.** 1995. Electromagnetic aircraft launch system – EMALS, *IEEE Transactions on Magnetics* 31(1): 528-533.
<http://dx.doi.org/10.1109/20.364638>.
2. **Marshall, R.; Ying, W.** 2004. Railguns: Their science and technology, China Machine Press, Beijing, China.
3. **Fair, H.D.** 2009. Advances in electromagnetic launch science and technology and its applications, *IEEE Transactions on Magnetics* 45(1): 225-230.
<http://dx.doi.org/10.1109/TMAG.2008.2008612>.
4. **Shvetsov, G.; Rutberg, P.; Budin, A.** 2007. Overview of some recent EML research in Russia, *IEEE Transactions on Magnetics* 43(1): 99-106.
<http://dx.doi.org/10.1109/TMAG.2006.887597>.
5. **Gallant, J.; Lehmann, P.** 2005. Experiments with brush projectiles in a parallel augmented railgun, *IEEE Transactions on Magnetics* 41(1): 188-193.
<http://dx.doi.org/10.1109/TMAG.2004.838988>.
6. **Daneshjoo, K.; Rahimzadeh, M., Ahmadi, R.; Ghassemi M.** 2007. Dynamic response and armature critical velocity studies in an electromagnetic railgun, *IEEE Transactions on Magnetics* 43(1): 136-131.
<http://dx.doi.org/10.1109/TMAG.2006.887668>.
7. **Liu, H.P.; Lewis, M.C.** 2009. 3-D electromagnetic analysis of armatures and rails for high launch, energy applications, *IEEE Transactions on Magnetics* 45(1): 322-326.
<http://dx.doi.org/10.1109/TMAG.2008.2008703>.
8. **Johnson, A.J.; Moon, F.C.** 2006. Elastic waves and solid armature contact pressure in electromagnetic launchers, *IEEE Transactions on Magnetics* 42(3): 422-429.
<http://dx.doi.org/10.1109/TMAG.2005.862105>.
9. **Johnson, A.J.; Moon, F.C.** 2007. Elastic waves in electromagnetic launchers, *IEEE Transactions on Magnetics* 43(1): 141-144.
<http://dx.doi.org/10.1109/TMAG.2006.887443>.
10. **Fryba, L.** 1999. *Vibration of Solids and structures Under Moving Loads*, Thomas Telford Ltd, London, p.494.
<http://dx.doi.org/10.1680/vosasuml.35393>.
11. **Tzeng, J.T.** 2003. Dynamic response of electromagnetic railgun due to projectile movement, *IEEE Transactions on Magnetics* 39(1): 472-475.
<http://dx.doi.org/10.1109/TMAG.2002.806384>.
12. **Tzeng, J.T.; Wei, S.** 2007. Dynamic response of cantilevered rail guns attributed to projectile/gun interaction – Theory, *IEEE Transactions on Magnetic* 43 (1): 207-213.
<http://dx.doi.org/10.1109/TMAG.2006.887444>.
13. **Nechitailo, N.V.; Lewis, B.K.** 2006. Critical velocity for rails in hypervelocity launchers, *Impact Engineering* 33(1-12): 485-495.
14. **Schneider, M.; Schneider, R.** 2008. Measurement of the current distribution between multiple brush armatures during launch, *IEEE Symposium on Electromagnetic Launch Technology*, 1-6.
<http://dx.doi.org/10.1109/ELT.2008.56>.
15. **Schneider, M.; Schneider, R.; Stankevič, V.; Balevičius, S.; Žurauskienė, N.** 2007. Highly local measurements of strong transient magnetic fields during railgun experiments using CMR-based sensors, *IEEE transactions on Magnetics* 43(1): 370-375.
<http://dx.doi.org/10.1109/TMAG.2006.887706>.
16. **Novickij, J.; Balevičius, S.; Žurauskienė, N.; Kačianauskas, R.; Stankevič, V.; Šimkevičius, Č.; Keršulis, S.; Bartkevičius S.** 2010. High magnetic field centre facilities, *Low Temp Physics* 159: 406-409.
<http://dx.doi.org/10.1007/s10909-009-0063-0>.
17. **Novickij, J.; Stankevič, V.; Balevičius, S.; Žurauskienė, N.; Cimperman, P.; Kačianauskas, R.; Stupak, E.; Kačianauskas, A.; Löffler, M.J.** 2006. Manganite sensor for measurements of magnetic field disturbances of pulsed actuators, *Solid State Phenomena* 113: 459-464.
18. **Kačianauskas, R.; Kačianauskas, A.; Stupak, E.; Balevičius, S.; Žurauskienė, N.; Novickij, J.** 2009. Numerical magneto-mechanical analysis of destructive coils with reinforcement cylinders having various thicknesses, *Acta physica polonica* 115(6): 1144-1145.
19. **Bartkevičius, S.; Novickij, J.** 2008. The investigation of stress distribution in pulsed magnets, *Electronics and Electrical Engineering* 87(7): 7-11.
20. **Tumonis, L.; Schneider, M.; Kačianauskas, R.; Kačianauskas, A.** 2009. Comparison of dynamic behaviour of EMA-3 railgun under differently induced loadings, *Mechanika* 78(4): 31-37.
21. **Tumonis, L.; Schneider, M.; Kačianauskas, R.; Vaidluga, V.** 2011. The structural mechanics of rail guns with discrete supports showing the influence of DES, *IEEE Transactions on Plasma Science* 39(1): 144-148.
<http://dx.doi.org/10.1109/TPS.2010.2072519>.

22. **Tumonis, L.; Kačianauskas, R.; Kačeniauskas, A.; Schneider, M.** 2007. The transient behaviour of rails used in electromagnetic railguns: numerical investigations at constant loading velocities, *Journal of Vibroengineering* 9(3): 15-17.
23. **Tumonis, L.; Schneider, M.; Kačianauskas, R.; Kačeniauskas, A.** 2009. Structural mechanics of railguns in the case of discrete supports, *IEEE Transactions On Magnetics* 45(1): 474-479. <http://dx.doi.org/10.1109/TMAG.2008.2008534>.
24. **Schneider, M.; Woetzel, M.; Wenning, W.; Walch, D.** 2009. The ISL rapid fire railgun project RAFIRA. Part I: Technical aspects and design considerations, *IEEE Transactions on Magnetics* 45(1): 442-447. <http://dx.doi.org/10.1109/TMAG.2008.2008468>.
25. **Schneider, M.; Woetzel, M.; Wenning, W.** 2009. The ISL rapid fire railgun project RAFIRA. Part II: first results, *IEEE Transactions on Magnetics* 45(1): 448-452. <http://dx.doi.org/10.1109/TMAG.2008.2008533>.
26. **ANSYS Theory Reference**, 12th edition, SAS IP INC., 2009.
27. **Kreivičius, A.; Juchnevičius, Ž.; Leonavičius, M.K.** 2010. The model of bent threaded connection in three segments, *Mechanika* 84(4): 5-11.

P. Gildutis, R. Kačianauskas, M. Schneider, E. Stupak, R. Stonkus

ELEKTROMAGNETINĖS ŠAUDYKLĖS SKERSINIO PJŪVIO DEFORMACIJŲ TYRIMAS

Reziumė

Apžvelgiami pirmieji Prancūzijos ir Vokietijos tyrimų instituto elektromagnetinės šaudyklės „Rafira“ skaitinio modeliavimo rezultatai. Tekste pateikiami paveikslai, lentelės, grafikai leidžia geriau suprasti deformuojamos šaudyklės skersinio pjūvio elgseną.

Konstrukcija sudaryta iš trimačių kompozicinių strypų ir plieninių varžtų. Straipsnyje baigtinių elementų metodu, naudojantis ANSYS programine įranga, nagrinėtas šaudyklės skerspjūvio poslinkių uždavinys, strypams taikant plokščiųjų deformacijų būvio savybes. Tirtos varžtų pailgėjimo, strypo lenkimo, bėgio įsiskverbimo į korpusą problemos, veikiant statinei ir dinaminei apkrovoms. Nustatyta, jog vertikaliai šaudyklės poslinkiui daugiausia įtakos turi varžtų pailgėjimas, o dinaminiai poslinkiai yra apie du kartus didesni už statinius poslinkius.

P. Gildutis, R. Kačianauskas, M. Schneider, E. Stupak, R. Stonkus

DEFORMATION ANALYSIS OF RAILGUN CROSS – SECTION

Summary

This paper presents the first results in a series of research efforts aiming to perform numerical modelling of the electromagnetic gun RAFIRA (RAPid FIRE RAilgun) of the French-German Research Institute of Saint-Louis (ISL). It deals with the understanding and the illustration of cross-sectional deformation behaviour.

The structure consists of the three-dimensional composite bars and connection bolts. In our approach the structure cross-section is considered as plane strain problem numerically solved by the finite element method. The influence of bolts elongation, transversal bending of bars and the rail-bar interaction is studied by solving the problem under static load and dynamic impulsive loads. It was found that the biggest vertical displacement of the railgun is produced by bolt elongation. In case of dynamic analysis, the results are approximately two times higher than the static analysis. The obtained results serve as the base for the future developments.

Keywords: railgun, cross-sectional deformation, dynamic analysis.

Received April 04, 2011

Accepted May 30, 2012